



## Needleless electrospinning for scaled-up production of ultrafine chitosan hybrid nanofibers used for air filtration

Lei Wang,<sup>a1</sup> Changbo Zhang,<sup>b1</sup> Feng Gao<sup>c\*</sup> and Gang Pan<sup>a,d\*</sup>

Received 00th January 20xx,  
Accepted 00th January 20xx

DOI: 10.1039/x0xx00000x

[www.rsc.org/](http://www.rsc.org/)

Large scale ultrafine chitosan hybrid nanofibers containing TiO<sub>2</sub> and/or Ag nanoparticles were prepared using needleless electrospinning method. The nanofiber production rate was reached 50 g/h by needleless electrospinning method, which was much higher than 0.02-1 g/h in the traditional single needle electrospinning method. By optimizing the spinning parameters, nanofibers with a smooth uniform morphology were obtained with diameters ranging from 25 to 60 nm and Ag nanoparticles with average size of 2.9 nm were deposited on the surface of the nanofibers without aggregation. The hybrid nanofibers exhibited a significant increase in filtration efficiency (> 99%) for removal of nanoparticles aerosol, comparable to commercial high-efficiency particulate air filters, but with lower pressure drop and less mess. The chitosan hybrid nanofibers showed excellent antibacterial activity, e.g. 97% of *E. coli* and 99% of *S. aureus* were killed within 2 h. The cross-linked nanofibers exhibited excellent water durability and maintained a stable microstructure in high humidity and in water immersion. The daily productivity can be achieved above 1.2 kg, which make this ultrafine nanofibers possible in the application of wound dressing, air filtration and environmental purification.

### Introduction

Air pollution, such as haze, is a serious human health concern in many developing nations.<sup>1, 2</sup> PM 2.5 is one of the most blatant serious sources of fine particulates in air and has been found to be the cause of many human diseases.<sup>3, 4</sup> Ultrafine particles, especially nanoparticles are more dangerous and not easy to filter out. There is an enormous requirement for clean air around the world which has sparked immense interest in the development of high efficiency filters. Nanofibrous materials have attracted increasingly attention in filtration.<sup>5-7</sup> Functional nanofibers are now recognized as efficient materials for the treatment of the environmental problems. Because of their unique properties of the electrospun nanofibers such as high surface area, high aspect ratio, good mechanical properties and the ability to incorporate multifunctional nanoparticles in the fibers, the resulting product can be an excellent filter medium for air and water contaminants purification.<sup>8-15</sup> The main difficulties focus on the high throughput, functionalization and fiber diameter reduction, while maintaining nanofibers stability.

Chitosan is recognized as the second most globally abundant natural polysaccharide after cellulose.<sup>16, 17</sup> Chitosan has several interesting properties including, biodegradability, nontoxicity and fungicidal effects, which make it an attractive material for uses in a wide range of industries.<sup>5, 18-26</sup> However, electrospinning of chitosan has proven to be difficult, because of the poor solubility of chitosan in water. Many researchers have investigated the effect of solvents on the morphology of chitosan nanofibers, such as, acetic acid, hydrochloric acid, formic acid and trifluoroacetic acid (TFA).<sup>27-30</sup> It has been found that increasing concentrations of chitosan cause the morphology of fibers to change from spherical beads to an interconnected fibrous network. Regardless, electrospun chitosan fiber has been prepared in solution with TFA or in a co-solvent system with TFA and dichloromethane.<sup>31, 32</sup> It is difficult to obtain large area homogenous fibers from chitosan solutions in pure TFA and the average fiber diameter is normally hundreds of nanometer with a broad distribution of fiber diameters. Furthermore, electrical sparks often occur, which can damage the samples and result in the defects to the chitosan nanofiber, including branched fibers and spindle or bead-like structures.<sup>33</sup> Nanofibers have been successfully electrospun from ionogenic polymers using mixed solutions of ionogenic polymer and non-ionogenic polymer. Electrospinning of chitosan nanofiber has been accomplished using a blend of chitosan with another polymer, such as poly (ethylene oxide) (PEO),<sup>34, 35</sup> poly (vinyl alcohol) (PVA),<sup>27, 31</sup> polyvinylpyrrolidone (PVP)<sup>36</sup> and silk fibroin.<sup>37</sup> Nevertheless, the obtained hybrid nanofibers normally have a large diameter. Decreasing the nanofiber diameter within these mats provides many beneficial effects such as increase specific surface area to volume ratios and decrease average pore size. The reported chitosan hybrid nanofibers was usually prepared using single needle electrospinning method, which was seriously restricted its scale-up production to meet the large-scale application. Recently, more attention has been paid to develop needleless electrospinning technique.<sup>38-41</sup>

<sup>a</sup> Department of Environmental Nanotechnology, Research Center for Eco-environmental Sciences, Chinese Academy of Sciences, 18 Shuangqing Road, Beijing 100085, P. R. China. Email: gpan@rcees.ac.cn

<sup>b</sup> Agro-Environmental Protection Institute, Ministry of Agriculture, Tianjin 300191, P. R. China

<sup>c</sup> National Center for Nanoscience and Technology, 11 Zhongguancun Beijiyitiao, Beijing 100190, P. R. China. Email: gaofeng@nanoctr.cn

<sup>d</sup> School of Animal, Rural and Environmental Sciences, Nottingham Trent University, Brackenhurst Campus, NG25 0QF, UK

† Co-first author with the same contribution to this work.

Electronic Supplementary Information (ESI) available: [details of any supplementary information available should be included here]. See DOI: 10.1039/x0xx00000x

The present work was aim to prepare the large scale freestanding ultrafine chitosan hybrid nanofibers mats by a home-made needleless electrospinning setup with high throughput. In this work, PVA, TiO<sub>2</sub> and/or Ag nanoparticles were introduced to improve the function and spinning ability, meanwhile reduce the fiber diameter. The production rate was compared with that of the single needle electrospinning. The performance of the nanofiber mats were investigated by using air filtration and antibacterial test. The test results indicated that the obtained hybrid nanofibers showed excellent antibacterial activity and a high filtration efficiency of nanoparticles aerosol with a low pressure drop while depositing a thin layer of nanofibers.

## Experimental

### Materials

Chitosan (CS) (B.R. grade, degree of deacetylation: 80.0-95.0%, MW: 590,000), Hydrochloric acid (37% of purity), Glutaraldehyde (50% in water) and Acetone were purchased from Sinopharm Chemical Reagent Co., Ltd. PVA (86-90% hydrolysed, MW: 118,000-124,000) was obtained from Zhong Ke Guo Chang Technology Co., Ltd (Beijing, China). Silver nitrite (AgNO<sub>3</sub>) and acrylic acid (AA) were purchased from Beijing Chemical Works. TiO<sub>2</sub> in the form of aeroxide hydrophilic fumed powder was purchased from Evonik Industries Metal Oxides. The polypropylene (PP) non-woven fabric (Thickness: 100 μm) was obtained from Handan Heng yong Protective & Clean Products Co., Ltd. (China). The high efficiency particulate air (HEPA) filter (CZU500W) was obtained from Chongqing Paper Industry Research and Design Institute Co., Ltd. (China). All chemicals were used without further purification.

### Needleless electrospinning of nanofiber mats

The home-made needleless electrospinning setup was used as described in Fig. 1, which was consisted of a positive stainless steel roller (length: 25 cm, diameter: 8 cm) connected with high voltage power supply (Spellman SL130 P300), a polytetrafluoroethylene solution tank (volume: 2 L) and a collect roller (length: 50 cm, diameter: 10 cm). The collect roller was placed vertically at the top of the spinning roller. The spinning roller was partially immersed in the spinning solution and the polymer solution could cover and load on the surface of rotatable roller during the electrospinning process. The rotation speed of spinning electrode was fixed at 20 rpm. The collector was rotating at a speed of 50 rpm. 4 wt% of chitosan solution was prepared by dissolving dry mass in 2% v/v aqueous acetic acid at room temperature then heating to 60°C with magnetic stirring for 24 h. 10 wt% of PVA solution was prepared by dissolving PVA polymer in deionized water at 60°C, and completely dissolved by stirring. Optimization of the electrospinning parameters were carried out by variation blend weight ratios (CS: PVA from 1/2 to 3/1), applied voltage (20–70 kV), the distance from the tip of the needle to grounded collector (TCD: 6–15 cm), AgNO<sub>3</sub> concentration (from 0.04% to 1.0%) and TiO<sub>2</sub> concentration (0.04%). The prepared mixed solutions were placed in a polytetrafluoroethylene solution tank. The electrospinning experiments were carried out at 25°C and 20% of relative humidity (RH). The nanofiber mats were collected on a grounded roller and dried at room temperature in vacuum for 24 h

to remove any remaining moisture or acetic acid. The nanofibers were cross-linked by placing them in a desiccator saturated with glutaraldehyde vapor for 24 h or with 4 wt% glutaraldehyde in acetone solution for 30 min.

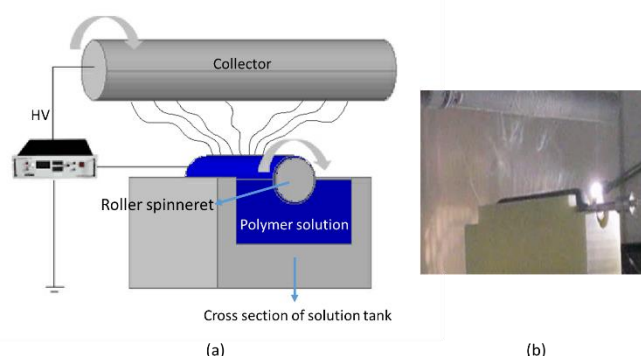


**Fig. 1** The diagram of needleless electrospinning setup (a) and the electrospinning process (b)

### Characterizations

The morphology of nanofiber was characterized by scanning electron microscope (SEM, S4800, HITACHI). The average nanofiber diameter was determined by the statistical treatment of the SEM images with Image J. The diameter distribution was obtained by measuring at minimum of 50 product nanofibers. Ag nanoparticles were characterized by transmission electron microscopy (TEM, Tecnai G2 20 S-TWIN, FEI) and energy dispersive X-ray spectroscopy (EDX). The conductivity of the spinning solution was measured by using a conductivity meter (DDS-11A, Shanghai REX Instrument Factory). Fourier transform infrared spectroscopy (FTIR) spectra of the chitosan nanofibers were performed in ATR mode from 4000 to 400 cm<sup>-1</sup> (Perkin-Elmer Spectrum 100).

### Testing of air filtration capacity

The CS hybrid nanofibers were deposited on the non-woven PP substrate which covered the collecting roller to form a composite filter. A TSI Automated Filter Tester (Model 8130) was used to measure the filtration performance of nanofibrous media. The testing particles were monodisperse solid NaCl aerosols with diameter of 75±20 nm. The testing time was 10 s with air flow of 32 L/min. The filtration efficiency (R) of nanoparticles aerosol was determined by the following equation:

$$R = (1 - C_p/C_0) \times 100\%$$

Where C<sub>p</sub> and C<sub>0</sub> represented the concentration of nanoparticles at the filter holder outlet with and without a filter installed. All of the tests were performed triplicate.

### Determination of antibacterial activity

The antibacterial properties against gram-negative *Escherichia coli* (*E. coli*) and gram-positive *Staphylococcus aureus* (*S. aureus*) of electrospun CS/PVA blends mats were tested using the agar plate method. Nanofiber samples were cut into wafers with diameter of 1 cm and then sterilized by ultraviolet radiation. After the activation, the prepared nanofiber samples were placed onto the agar plate where the bacteria was inoculated and cultured at 37°C for 24 h. Photographs were used to illustrate the antibacterial performance of the samples.

The shake flask method was used to test the bactericidal kinetics of the CS hybrid nanofiber. The initial concentration of bacteria was  $7 \times 10^6$  CFU/mL. 20 mg of CS hybrid nanofiber mat was put into 50 mL of bacteria solution, which was kept on shaking at 37°C. 0.1 mL of the bacteria solution was sampled every 0.5 h and cultured on an agar plate at 37°C for one day. Control experiment was carried out without adding the CS hybrid nanofiber mats and the bacterial colonies were counted. The bactericidal kinetics were determined by the degradation of bacterial colonies. All of the experiments were performed triplicate.

## Results and discussion

### Characterization of chitosan hybrid nanofiber mats

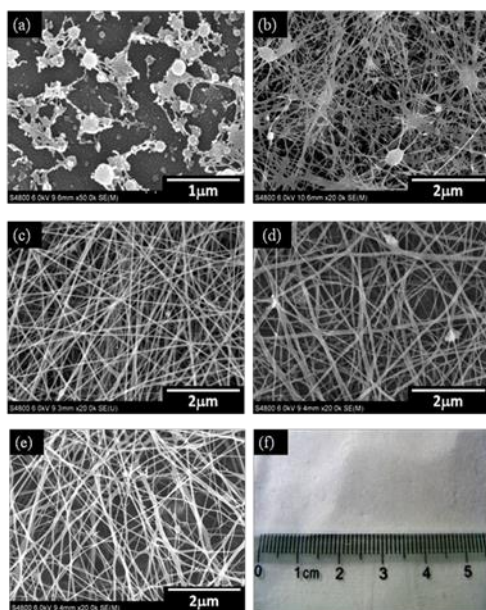


**Fig. 2** FE-SEM images of various nanofibers (a) CS, (b) CS/PVA, (c) CS/PVA/Ag, (d) CS/PVA/TiO<sub>2</sub>, (e) CS/PVA/Ag/TiO<sub>2</sub> and (f) optical image of part nanofiber mat. The concentration of AgNO<sub>3</sub> was 0.1% and TiO<sub>2</sub> was 0.04%.

Needleless electrospinning was performed by a home-made setup with an applied voltage of 50 kV and collection distance of 10 cm. Electrospinning of CS in 2% acrylic acid solution over a broad concentration range failed to yield the desired nanofibers. As shown in Fig. 2a, the bead structure was formed during the electrospinning process. Chitosan nanofibers can't be directly prepared by the electrospinning method,<sup>42</sup> because of its natural properties such as low solubility, high degree of inter and intra-chain hydrogen bonding. It has been found that the addition of a non-ionogenic polymer with a flexible chain could facilitate the nanofiber formation of the CS

from ionogenic polymers. PVA has good fiber-forming ability and biocompatibility, so it was selected as the suitable non-ionogenic partner for preparation of CS hybrid nanofibers.<sup>43, 44</sup> From Fig. 2b, PVA obviously enhanced the electrospinning ability of CS and improved the material properties of chitosan resulting in, for example, high tensile strength.<sup>45</sup>

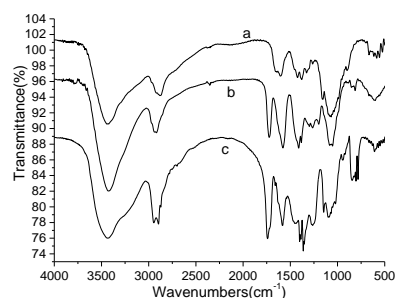


**Fig. 3** FTIR spectra of the electrospun nanofiber mats (a) CS, (b) CS/PVA and (c) PVA.

Fig. 3 summarizes the FTIR spectra of various nanofiber mats. The presence of CS in the mat was confirmed by the absorption bands for O-H and N-H at 3441 cm<sup>-1</sup>, the saccharine characteristic peak around 1150 cm<sup>-1</sup>-898 cm<sup>-1</sup> and an amino peak at 1255 cm<sup>-1</sup>. It was observed that O-H and N-H stretching vibrations shifted to a lower wavenumber and the amino peak at 1255 cm<sup>-1</sup> disappeared in the CS/PVA nanofibers. Moreover, N-H peak at 1580 cm<sup>-1</sup> and the saccharine characteristic peaks were present in CS/PVA nanofibers. These results indicated that CS and PVA formed hydrogen bonds and the repulsive force between the ionic groups within the CS backbone decreased which improved the electrospinning ability of CS. However, the morphology of the CS/PVA nanofiber mat was still included some beads structure and the fibers were not uniform in the diameter (Fig. 2b). The CS/PVA blend nanofibers with AgNO<sub>3</sub> and/or TiO<sub>2</sub> were successfully fabricated with a uniform smooth morphology and ultrafine diameters in range of 25-60 nm (Fig. 2c-e), which were much lower than the reported chitosan nanofibers with diameters of 90-220 nm prepared by single needle electrospinning method.<sup>42, 46, 47</sup> The conductivity of the various CS, CS/PVA, CS/PVA/AgNO<sub>3</sub> and CS/PVA/TiO<sub>2</sub> hybrid solutions were 2.24, 3.06, 3.66 and 3.25 mS/cm, respectively. This result suggested that the conductivity of the solution played an important role in the electrospinning and the addition of AgNO<sub>3</sub> and TiO<sub>2</sub> significantly improved the electrospinning capability of the CS/PVA solution.

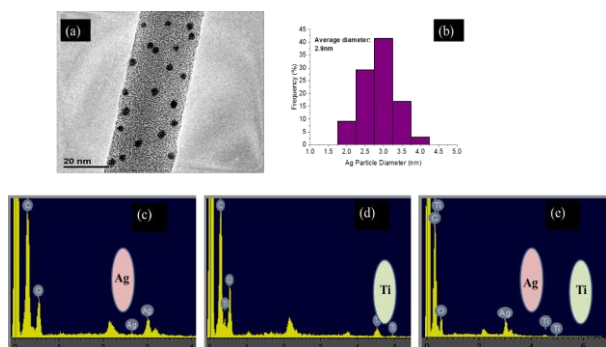


**Fig. 4** (a) TEM image of the CS hybrid nanofiber mats and (b) the diameter distribution of the Ag nanoparticles. The EDX spectra of different hybrid nanofibers (c) CS/PVA/Ag, (d) CS/PVA/TiO<sub>2</sub> and (e) CS/PVA/Ag/TiO<sub>2</sub>. The other peaks on the spectra were attributed to Au due to the Au coating performing.

Fig. 4a presents the TEM images of the nanofibers and it clearly shows that the Ag nanoparticles with an average diameter around of 2.9 nm are successfully deposited on the surface of nanofibers (Fig. 4b). Nanosized Ag particles offer high reaction activity, such as catalysis and antibacterial activity.<sup>48, 49</sup> Various blended fibers with Ag and/or TiO<sub>2</sub> were synthesized with uniform morphologies and ultrafine fiber diameters. The deposition of Ag and TiO<sub>2</sub> in the mats were further verified using energy dispersive X-ray spectroscopy analysis, as shown in Fig. 4c-e.

#### Systematic effects on the preparation of CS hybrid nanofibers

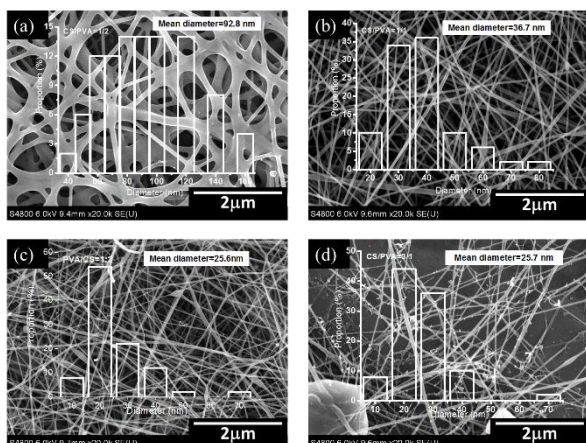


**Fig. 5** FE-SEM images and diameter distribution of the CS/PVA/Ag mats with different CS to PVA weight ratios (a) 1/2, (b) 1/1, (c) 2/1 and (d) 3/1. The AgNO<sub>3</sub> concentration was 0.1%.

In order to obtain the high quality of nanofibers, electrospinning parameters was optimized by using CS/PVA/Ag as an example. Applied voltage and collection distance were 50 kV and 10 cm, respectively. Fig. 5 shows the SEM micrographs of the subject fibrous mat. This figure reveals the average diameter and diameter distribution of the CS/PVA/Ag hybrid nanofiber mats containing 0.1% AgNO<sub>3</sub> with different weight ratios of CS/PVA. As shown in Fig. 5b, a uniform nanofibers structure was observed when the CS/PVA weight ratio was 1/1. The nanofiber diameter gradually decreased with the increase of CS content in the blend solution. For example, the diameter of the fibers with a CS/PVA weight ratio of 1:2 was 92.8 nm, but this diameter decreased to 25.7 nm when the ratio of CS/PVA

was 3/1. This result can be explained by the increase of charge density of the spinning solution and the increase of conductivity as the increase of CS content in the solution (Table 1).<sup>27</sup> However, when the CS/PVA weight ratio reached up to 3/1, few nanofibers were resulted. An increase in the amount of nanofiber defects were also observed, such as branched fibers, bead-like structures. This result was possibly due to the increase of CS content in the spinning solution, which could induce the increase of repulsive force between the ionic groups within the polymer's backbone. This was detrimental to continuous fiber formation under high electric field.

The effect of the AgNO<sub>3</sub> concentration in the mixture was also investigated. From the results shown in Fig. 6, the nanofibers were successfully synthesized with various concentrations of AgNO<sub>3</sub> (0.04%, 0.1%, 0.5% and 1.0%) and all of the resulting nanofibers exhibited a smooth morphology and uniform diameter. It can be concluded from these results that the addition of Ag ions significantly improved the spinning ability of the CS/PVA solution. The conductivity of the solution was increased from 3.37 to 6.60 mS/cm when the AgNO<sub>3</sub> concentration was increased from 0 to 1.0% (Table 1). However, the average diameter of the fibers increased from 34.5 to 61.7 nm under the same circumstances, which was inconsistent with the increase in the AgNO<sub>3</sub> concentration. The possible reason for this latter result was that as the AgNO<sub>3</sub> concentration in solution increased, the dynamic viscosity of solution increased, which was unfavorable for the electrospinning process. Nanofibers with ultrafine diameter were desired, so the concentration of AgNO<sub>3</sub> was controlled from 0.04% to 0.1% in this study. From the above results, it appeared that the surface morphology of the nanofibers and the average fiber diameters were significantly affected by the composition of the spinning solution.

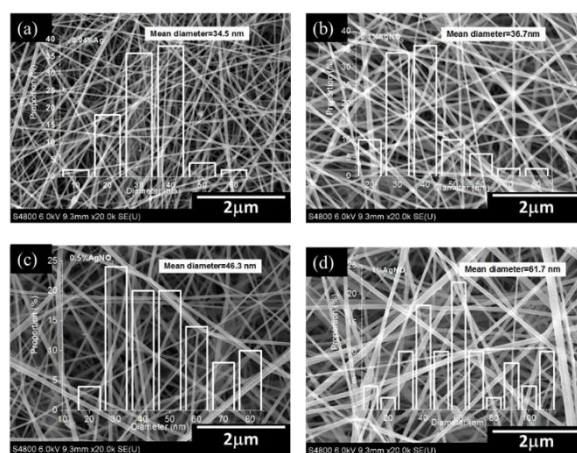


**Fig. 6** FE-SEM images and diameter distribution of the CS/PVA/Ag mats with different AgNO<sub>3</sub> concentrations (a) 0.04%, (b) 0.1%, (c) 0.5% and (d) 1.0%. CS to PVA weight ratio was 1/1.

**Table 1** Conductivity ( $\sigma$ ) of the mixed solutions under different conditions.

Conditions	Different CS/PVA(w/w) (0.1%AgNO <sub>3</sub> )				Different AgNO <sub>3</sub> content (CS/PVA=1/1)				
	1/2	1/1	2/1	3/1	0	0.04%	0.1%	0.5%	1.0%
$\sigma$ (mS/cm)	3.56	3.66	3.76	3.83	3.37	3.43	3.66	4.62	6.60

**Table 2** Voltage and TCD effects on the fiber diameter.

<sup>(a)</sup> Voltage/kV	20	30	50	60	70
$d_{ave}/nm$	60.5	45.0	36.7	38.5	40.0
<sup>(b)</sup> TCD/cm	6	9	10	12	15
$d_{ave}/nm$	45.5	37.0	36.7	44.2	48.4

It has been reported that applied voltage has an important effect on the synthesis of the electrospun nanofibers and especially affects the fiber diameter and the morphology.<sup>32, 33</sup> To determine the effect of applied voltage, a series of experiments were conducted where the conditions were, a ratio of CS/PVA 1/1, 0.1% AgNO<sub>3</sub> and TCD (tip to collector distance) was 10 cm. The applied voltage was varied from 20 to 70 kV. Within these applied voltages the resulting nanofibers were produced with a smooth morphology. The results in Table 2a, appear to suggest that the average diameter of nanofibers decreased with the increase of the applied voltage, which was in accordance with results reported by Sencadas et al.<sup>32</sup> But when applied voltage was too high, the phenomenon of electrical sparking often occurred during the spinning process which induced the discontinuous spinning of the nanofibers. This adversely affected the morphology and diameter of the fibers. Table 2b shows the TCD effects on the fiber diameter. These results suggested that the fiber diameter increased as the TCD increased from 9 to 15 cm. This was due to weak dissipative forces that occurred at longer TCD. The same result was observed with a lower TCD (below 9 cm), the explanation for this could be that short distance adversely affected the solvent evaporation, inducing more adhesion between the nanofibers resulting in the formation of large diameter fibers. Therefore, it is important to optimize the applied voltage and distance during the electrospinning process. Using a TCD of 10 cm and 50 kV, smooth nanofibers were produced with an average diameter of 36.7 nm.

Applied voltage effect on the production rate of CS hybrid nanofiber was measured in this study. The most important thing of electrospinning was keeping on a continuous fluent electrospinning process. The production rate of nanofibers were achieved 28, 50 and 36.5 g/h when the applied voltage was tested at 20, 50 and 70 KV, separately. The maximum productivity was obtained at 50 KV. When the voltage was low, the amount of jet flow was less than that of high voltage, but when the applied voltage was too high, the phenomenon of electrical sparking often occurred and thus caused the discontinuous electrospinning and low productivity. Herein, the productivity of ultrafine chitosan hybrid nanofibers could be achieved 50 g/h by using the home-made needleless electrospinning setup (50 KV, TCD: 10 cm). Thus, the daily production rate was reached over 1.2 kg in bench-scale laboratory test. However, the production rate of the known single-needle electrospinning was limited to 0.02-1 g/h.<sup>39</sup> This work provided an efficient approach for massive production of high quality functional nanofibers and the production could be further improved in pilot scale test.

#### Cross-linking of electrospun nanofibers

To improve the potential application of the subject nanofibers in the aqueous environments, we chose to cross-link the polymers to improve the durability of the nanofibers in water. Glutaraldehyde vapor and glutaraldehyde solution were all studied and compared in

this work. Control experiments were performed using nanofibers without any treatment. All samples were immersed in deionized water for 30 min. As shown in Fig. 7, when the electrospun nanofiber mats were immersed in water solution, they were disintegrated instantaneously and the fibers dissolved with neither the mat nor individual fibers remaining intact. Cross-linking the fibers using glutaraldehyde vapor improved their water durability of the product. However, the morphology of mats and the porous structure were still partially destroyed. From all of the SEM images, it was evident that after cross-linking with 4% glutaraldehyde solution the fiber mats became highly water durable and maintained their integrity as long, randomly oriented, cylindrical fibers (Fig. 7c). The glutaraldehyde residue was removed by washing with water for several times and drying under vacuum condition to remove the remaining solvent. Nanofibers cross-linked by glutaraldehyde solution retained their shape and rigidity unaltered in an environment of high humidity or water immersion.

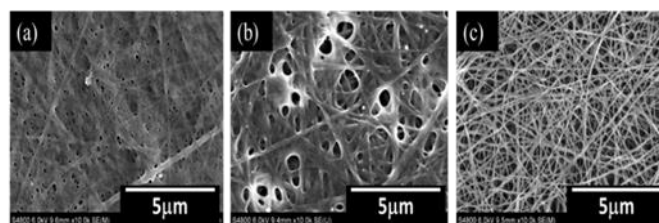


**Fig. 7** FE-SEM images of the CS/PVA/Ag nanofiber mats immersed in water for 30 min: (a) without treatment, (b) cross-linked using glutaraldehyde vapor and (c) cross-linked using 4% glutaraldehyde solution.

#### Air filtration performances of the chitosan hybrid nanofiber filters

Fig. 8 (a) shows the filtration efficiency and pressure drop across of composite membrane versus the thickness of nanofibers. The PP fabrics have large pore size about 10 μm and high diameter of 2 μm. The filtration efficiency of PP non-woven fabrics was only 17.0%, but it was increased significantly and achieved above 98% after compositing with a thin layer of CS hybrid nanofibers. The filtration efficiency of ultrafine nanoparticles were effected by mechanisms of Brownian diffusion and electrostatic absorption, which was different from the large size particles by interception. Nanoparticles were easily captured on the surface of the nanofiber layer due to its ultrafine diameter and small pore size (Fig. 8). The filtration efficiency increased from 17.0% to 99.2% with the increase of the thickness of the nanofibers layer from 0 to 18.7 μm and then decreased a little to 98.4% in the case of the 27.4 μm fibers. The filtration efficiencies were significantly improved with the addition of a thin layer of CS hybrid nanofibers (only 2.5 μm). The pressure drop was also increased along with the increase in fiber thickness. Filtration experiment was also carried using a commercial high-efficiency particulate air (HEPA) filter. The HEPA showed the filtration efficiency of 99.95%, but with a much higher pressure drop of 280 mm H<sub>2</sub>O than that of the chitosan composite nanofibers filter media (Fig. 8). High efficient filters normally need both higher filtration efficiency and lower pressure drop. It can be concluded that the chitosan composite

filter media presented better performance than HEPA for the filtration of nanoparticles aerosol.

In order to study the nanoparticles aerosol filtration efficiency based on the size of the nanofibers, the filtration efficiency of CS hybrid nanofibers with different nanofiber diameters were tested. As shown in Fig. 9, with increasing nanofiber diameter the air filtration efficiency was decreased. In this work, the ultrafine nanofibers (tens of nm) showed significant improvement in the aerosol nanoparticles filtration compared with the reported fibers with hundreds of nm or micrometer diameter.<sup>50–51</sup> It was attributed to the higher pore size obtained with increasing nanofiber diameters along with increase in air permeability.

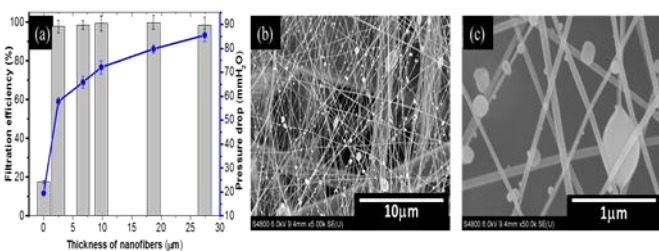


**Fig. 8** The filtration efficiency and pressure drop of nanofibers versus the thickness of nanofibers (a) and the SEM images of the samples after filtrating aerosols with (b) low scale and (c) magnified scale.

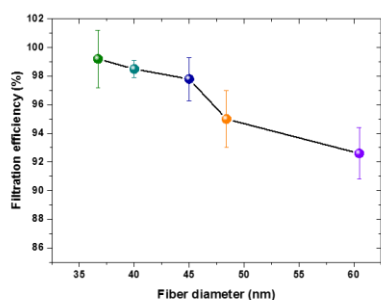


**Fig. 9** The filtration efficiency of nanofibers with different diameters

#### Antibacterial activity of the nanofiber mats

During the filtration process, especially the indoor filtration, the pathogenic organisms normally can stay on the surface of filters. The growth and proliferation of bacteria on the filters can result in the decrease of filtration efficiency and improve the pathogenic risk. Thus, it is important to prepare the antibacterial membrane filter. The antimicrobial properties of the synthesized fiber mats were determined using *E. coli* and *S. aureus* which were inoculated with CS/PVA/Ag or CS/PVA/TiO<sub>2</sub> nanofiber membrane on agar plates for 24 h. Controls consisted of a PVA membrane and CS/PVA nanofiber membrane which were also inoculated with these bacteria and grown on agar plates for 24 h. Based on the results for the inhibition zone of the circle shown in Fig. 10, the nanofiber mats with Ag or TiO<sub>2</sub> exhibited evident antibacterial activity. The CS/PVA also inhibited the growth of the bacteria, because chitosan has antibacterial properties, caused by damaging the interaction of polycations with the negatively charged surface of the bacteria and thus result in a loss of

membrane permeability, cell leakage and cell death. Fig. 10a-d shows the lesions and holes on the bacterial cell membrane, which indicate the damages of the bacterial cell caused by the CS/PVA/Ag nanofiber mats. The shake flask method was used to examine the bactericidal kinetics of the nanofiber mats. 20 mg of CS/PVA/Ag or CS/PVA/TiO<sub>2</sub> nanofibers were added to tubes containing 50 mL of the test bacteria at a concentration of  $7 \times 10^6$  CFU/mL. The tubes were maintained in an incubated shaker at 37°C. Fig. 10e shows the bactericidal kinetics of the CS hybrid nanofiber mats with Ag or TiO<sub>2</sub>. Both types of nanofibers exhibited powerful antibacterial activity. The antibacterial activity of the nanofibers with 0.04% AgNO<sub>3</sub> attained a mortality rate of 97% for *E. coli* and 99% for *S. aureus* within 2 h. The nanofibers with 0.04% TiO<sub>2</sub> exhibited a mortality rate of 90% for *E. coli* and 92% for *S. aureus*. The Ag nanoparticle presented strong bactericidal activity, because it could affect the cell wall permeability and cellular respiration.<sup>52–54</sup> TiO<sub>2</sub> will naturally be more effective bactericidal under irradiation. However, these results suffice to show that the CS hybrid nanofibers with Ag or TiO<sub>2</sub> are excellent antibacterial materials. The presence of micro- and nano-sized pores in the same antibacterial membrane not only performs acceptable filtration while assisting to minimize microbial fouling. Consequently, this novel filtration medium can be used for simultaneous nanoparticles filtration and disinfection of pathogens, such as viruses and bacteria.

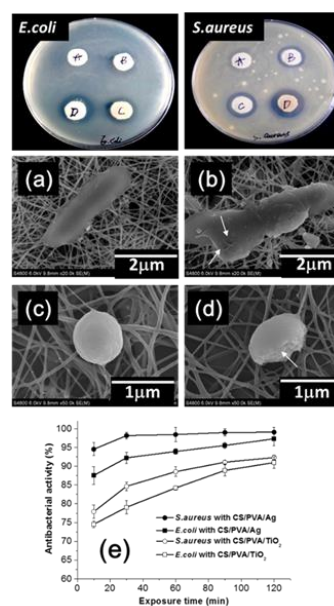


**Fig. 10** Images of the inhibition zone of various fibers (A) PVA, (B) CS/PVA, (C) CS/PVA/TiO<sub>2</sub> and (D) CS/PVA/Ag; SEM images of *E. coli* and *S. aureus* contacted with CS/PVA/Ag nanofiber (a, c) 0 h and (b, d) 2 h and (e) the bactericidal kinetics. The test was carried out in  $7 \times 10^6$  CFU/mL of *E. coli* and *S. aureus*.

#### Conclusions

In conclusion, for the first time, high throughput non-woven mats of chitosan hybrid nanofibers containing TiO<sub>2</sub> and/or Ag nanoparticles were prepared using needleless electrospinning method. Needleless electrospinning significantly improved the production rate of chitosan hybrid nanofibers, which was more

than 50 fold higher than the yields in the traditional single needle electrospinning method. The daily productivity could be achieved above 1.2 kg. Through optimization of the spinning conditions, the ultrafine chitosan hybrid nanofibers with the diameters ranging from 25 to 60 nm were obtained in this work. When the nanofiber mats were cross-linked using 4% glutaraldehyde solution, they exhibited excellent water durability and maintained their original morphology in an environment of high humidity or when immersed in water. The hybrid nanofibers mats exhibited high filtration efficiency of nanoparticles aerosol and excellent antibacterial activity. In addition, with the presence of an abundance of functional groups, the large scale ultrafine CS hybrid nanofibers could be used as a nanoreactor system to produce fiber-based composite nanostructured materials. The porous structures of these materials could make them useful for applications ranging from wound dressing, filtration to environmental remediation.

## Acknowledgements

This work was supported by National Natural Science Foundation of China (21407160), Natural Science Funds Fund form Tianjin (13JCYBJC20300), Strategic Priority Research Program of the Chinese Academy of Sciences (XDA09030203) and the Science Promotion Programme of Research Center for Eco-environmental Sciences, CAS (YSW2013B05).

## Notes and references

- D. Ji, Y. Wang, L. Wang, L. Chen, B. Hu, G. Tang, J. Xin, T. Song, T. Wen, Y. Sun, Y. Pan and Z. Liu, *Atmospheric Environment*, 2012, **50**, 338-348.
- J. Ma, X. Xu, C. Zhao and P. Yan, *Advances in Atmospheric Sciences*, 2012, **29**, 1006-1026.
- A. Wei and Z. Meng, *Environmental Toxicology and Pharmacology*, 2006, **22**, 292-297.
- L. Nikasinovic, J. Just, F. Sahraoui, N. Seta, A. Grimfeld and I. Momas, *Journal of Allergy and Clinical Immunology*, 2006, **117**, 1382-1388.
- H. Deng, P. Lin, W. Li, S. Xin, X. Zhou and J. Yang, *Journal of Biomaterials Science-Polymer Edition*, 2013, **24**, 485-496.
- B. Ding, E. Kimura, T. Sato, S. Fujita and S. Shiratori, *Polymer*, 2004, **45**, 1895-1902.
- A. Greiner and J. H. Wendorff, *Angewandte Chemie-International Edition*, 2007, **46**, 5670-5703.
- J. Li, F. Gao, L. Q. Liu and Z. Zhang, *Express Polymer Letters*, 2013, **7**, 683-689.
- Q. Li, Y. Xu, H. Wei and X. Wang, *RSC Advances*, 2016, **6**, 65275-65281.
- Y. Yang, S. Zhang, X. Zhao, J. Yu and B. Ding, *Separation and Purification Technology*, 2015, **152**, 14-22.
- K. Liu, Z. Xiao, P. Ma, J. Chen, M. Li, Q. Liu, Y. Wang and D. Wang, *RSC Advances*, 2015, **5**, 87924-87931.
- W. Jang, J. Yun, K. Jeon and H. Byun, *RSC Advances*, 2015, **5**, 46711-46717.
- D. Xu, S. Yan, W. weng and R. Xiao, *RSC Advances*, 2016, **6**, 44723-44731.
- W. Ma, Q. Zhang, D. Hua, R. Xiong, J. Zhao, W. Rao, S. Huang, X. Zhan, F. Chen and C. Huang, *RSC Advances*, 2016, **6**, 12868-12884.
- J. Wang, K. Pan, E. P. Giannelis and B. Cao, *RSC Advances*, 2013, **3**, 8978-8987.
- A. M. El-Shafei, M. M. G. Fouda, D. Knittel and E. Schollmeyer, *Journal of Applied Polymer Science*, 2008, **110**, 1289-1296.
- A. Hebeish, F. A. Abdel-Mohdy, M. M. G. Fouda, Z. Elsaid, S. Essam, G. H. Tammam and E. A. Drees, *Carbohydrate Polymers*, 2011, **86**, 1684-1691.
- R. Hejazi and M. Amiji, *Journal of Controlled Release*, 2003, **89**, 151-165.
- M. Dash, F. Chiellini, R. M. Ottenbrite and E. Chiellini, *Progress in Polymer Science*, 2011, **36**, 981-1014.
- N. Bhardwaj and S. C. Kundu, *Biotechnology Advances*, 2010, **28**, 325-347.
- H. Deng, X. Li, B. Ding, Y. Du, G. Li, J. Yang and X. Hu, *Carbohydrate Polymers*, 2011, **83**, 973-978.
- H. Deng, P. Lin, S. Xin, R. Huang, W. Li, Y. Du, X. Zhou and J. Yang, *Carbohydrate Polymers*, 2012, **89**, 307-313.
- F. Ding, H. Deng, Y. Du, X. Shi and Q. Wang, *Nanoscale*, 2014, **6**, 9477-9493.
- W. Huang, H. Xu, Y. Xue, R. Huang, H. Deng and S. Pan, *Food Research International*, 2012, **48**, 784-791.
- R. Xu, S. Xin, X. Zhou, W. Li, F. Cao, X. Feng and H. Deng, *International journal of pharmaceutics*, 2012, **438**, 258-265.
- M. N. V. Ravi Kumar, *Reactive and Functional Polymers*, 2000, **46**, 1-27.
- L. Li and Y. L. Hsieh, *Carbohydrate Research*, 2006, **341**, 374-381.
- X. Y. Geng, O. H. Kwon and J. H. Jang, *Biomaterials*, 2005, **26**, 5427-5432.
- P. Sangsanoh and P. Supaphol, *Biomacromolecules*, 2006, **7**, 2710-2714.
- J. D. Schiffman and C. L. Schauer, *Polym. Rev.*, 2008, **48**, 317-352.
- K. Ohkawa, D. I. Cha, H. Kim, A. Nishida and H. Yamamoto, *Macromolecular Rapid Communications*, 2004, **25**, 1600-1605.
- V. Sencadas, D. M. Correia, A. Areias, G. Botelho, A. M. Fonseca, I. C. Neves, J. L. G. Ribelles and S. L. Mendez, *Carbohydr. Polym.*, 2012, **87**, 1295-1301.
- A. C. Areias, J. A. Gomez-Tejedor, V. Sencadas, J. Alio, J. L. Gomez Ribelles and S. Lanceros-Mendez, *Polym. Eng. Sci.*, 2012, **52**, 1293-1300.
- B. Duan, C. H. Dong, X. Y. Yuan and K. D. Yao, *Journal of Biomaterials Science-Polymer Edition*, 2004, **15**, 797-811.
- N. Bhattarai, D. Edmondson, O. Veis, F. A. Matsen and M. Q. Zhang, *Biomaterials*, 2005, **26**, 6176-6184.
- L. Zhang, X. Bai, H. Tian, L. Zhong, C. Ma, Y. Zhou, S. Chen and D. Li, *Carbohydrate Polymers*, 2012, **89**, 1060-1066.
- W. H. Park, L. Jeong, D. I. Yoo and S. Hudson, *Polymer*, 2004, **45**, 7151-7157.
- D. Z. Wu, X. P. Huang, X. T. Lai, D. H. Sun and L. W. Lin, *Journal of Nanoscience and Nanotechnology*, 2010, **10**, 4221-4226.
- X. Wang, X. W. Hu, X. C. Qiu, X. Y. Huang, D. Z. Wu and D. H. Sun, *Materials Letters*, 2013, **99**, 21-23.
- D. W. Li, T. Wu, N. F. He, J. Wang, W. M. Chen, L. P. He, C. Huang, H. A. Ei-Hamshary, S. S. Al-Deyab, Q. F. Ke and X. M.

- Mo, *Colloids and Surfaces B-Biointerfaces*, 2014, **121**, 432-443.
41. K. Molnar and Z. K. Nagy, *European Polymer Journal*, 2016, **74**, 279-286.
42. Y. Zhou, D. Yang and J. Nie, *Journal of Applied Polymer Science*, 2006, **102**, 5692-5697.
43. V. Gimenez, A. Mantecon and V. Cadiz, *Journal of Polymer Science Part a-Polymer Chemistry*, 1996, **34**, 925-934.
44. M. Krumova, D. Lopez, R. Benavente, C. Mijangos and J. M. Perena, *Polymer*, 2000, **41**, 9265-9272.
45. T. T. T. Nguyen, B. Tae and J. S. Park, *Journal of Materials Science*, 2011, **46**, 6528-6537.
46. L. L. Min, Z. H. Yuan, L. B. Zhong, Q. Liu, R. X. Wu and Y. M. Zheng, *Chemical Engineering Journal*, 2015, **267**, 132-141.
47. A. Esmaeili and A. A. Beni, *Journal of Hazardous Materials*, 2014, **280**, 788-796.
48. C. N. Lok, C. M. Ho, R. Chen, Q. Y. He, W. Y. Yu, H. z. Sun, P. K. H. Tam, J. F. Chiu and C. M. Che, *J. Biol. Inorg. Chem.*, 2007, **12**, 527-534.
49. E. Navarro, F. Piccapietra, B. Wagner, F. Marconi, R. Kaegi, N. Odzak, L. Sigg and R. Behra, *Environ. Sci. Technol.*, 2008, **42**, 8959-8964.
50. K. Desai, K. Kit, J. Li, P. M. Davidson, S. Zivanovic and H. Meyer, *Polymer*, 2009, **50**, 3661-3669.
51. X. H. Qin and S. Y. Wang, *Journal of Applied Polymer Science*, 2006, **102**, 1285-1290.
52. J. Song, H. Kang, C. Lee, S. H. Hwang and J. Jang, *Acs Applied Materials & Interfaces*, 2012, **4**, 460-465.
53. S. j. Yu, J. b. Chao, J. Sun, Y. g. Yin, J. f. Liu and G. b. Jiang, *Environmental Science & Technology*, 2013, **47**, 3268-3274.
54. J. Liu and R. H. Hurt, *Environmental Science & Technology*, 2010, **44**, 2169-2175.